AIP | Journal of Applied Physics

Electrical and optical characterization of Au/CaF2/p-Si(111) tunnel-injection diodes

Yu. Yu. Illarionov, M. I. Vexler, V. V. Fedorov, S. M. Suturin, and N. S. Sokolov

Citation: Journal of Applied Physics **115**, 223706 (2014); doi: 10.1063/1.4882375
View online: http://dx.doi.org/10.1063/1.4882375
View Table of Contents: http://scitation.aip.org/content/aip/journal/jap/115/22?ver=pdfcov
Published by the AIP Publishing

Articles you may be interested in

Electrical characterization and modeling of the Au / CaF 2 / n Si (111) structures with high-quality tunnel-thin fluoride layer
J. Appl. Phys. **105**, 083716 (2009); 10.1063/1.3110066

Room temperature negative differential resistance of Cd F 2 Ca F 2 double-barrier resonant tunneling diode structures grown on Si(100) substrates
Appl. Phys. Lett. **90**, 092101 (2007); 10.1063/1.2709508

Ca F 2 Si Ca F 2 resonant tunneling diodes grown by B surfactant-mediated epitaxy
Appl. Phys. Lett. **86**, 033111 (2005); 10.1063/1.1853522

Resonant tunneling characteristics in SiO 2 / Si double-barrier structures in a wide range of applied voltage
Appl. Phys. Lett. **83**, 1456 (2003); 10.1063/1.1603352

Hot-electron transport through Au/CaF 2 /Si (111) structure studied by ballistic electron emission spectroscopy
J. Appl. Phys. **85**, 941 (1999); 10.1063/1.369214

AIP | Journal of Applied Physics

Journal of Applied Physics is pleased to announce André Anders as its new Editor-in-Chief

[This article is copyrighted as indicated in the article. Reuse of AIP content is subject to the terms at: http://scitation.aip.org/termsconditions. Downloaded to] IP: 128.131.199.82 On: Thu, 10 Jul 2014 10:07:53

Electrical and optical characterization of Au/CaF_2/p-Si(111) tunnel-injection diodes

Yu. Yu. Illarionov,[1,2,3,a] M. I. Vexler,[2] V. V. Fedorov,[2] S. M. Suturin,[2] and N. S. Sokolov[2]
[1]*Singapore Institute of Manufacturing Technology, 71 Nanyang Drive 638075, Singapore*
[2]*Ioffe Physical-Technical Institute, 26 Polytechnicheskaya Str., 194021 St.-Petersburg, Russia*
[3]*TU Vienna, Institute for Microelectronics, 27-29 Gusshausstr., 1040 Vienna, Austria*

(Received 5 January 2014; accepted 29 May 2014; published online 10 June 2014)

Metal/CaF_2/p-Si(111) capacitors with the improved-quality several-nanometer-thick epitaxial fluorite films are examined, aiming at solidifying a candidacy of this material for barrier layers in silicon devices. Structural and transport properties of a thin crystalline dielectric are characterized by different experimental techniques. The measured current-voltage characteristics accompanied with simulation results demonstrate that the elastic tunneling electron injection takes place in the considered structures. The same result follows from the behavior of hot-electron-injection-related electroluminescence within the selected spectral intervals. The result is important considering a perspective of using the epitaxial fluorides as barrier layers in resonant tunneling diodes. © *2014 AIP Publishing LLC*. [http://dx.doi.org/10.1063/1.4882375]

I. INTRODUCTION

Calcium fluoride (CaF_2) is a relatively new insulating material with a high dielectric constant ($\varepsilon = 8.43$) and a wide bandgap (12.1 eV). CaF_2 layers are typically grown by molecular beam epitaxy (MBE) and a considerable progress in understanding of the growth processes and electrophysical properties has been achieved recently.[1,2] Thin calcium fluoride films are intended to be applied as the insulating barrier layers in silicon solid state devices, such as Resonant-Tunneling Diodes (RTDs) and super-lattices employing Si,[3] CdF_2,[4] or Fe_3Si (Ref. 5) quantum wells. These devices can exhibit higher peak-to-valley current ratio than the conventional $A^{III}B^{V}$-compound based systems. Furthermore, the Fe_3Si/CaF_2 RTDs may serve as spin injectors.[6] Not to exclude is also a revival of an idea[7] of employing thin fluoride as a gate dielectric in the conventional Field-Effect Transistors (FETs).

However, the quality of the MBE-grown CaF_2 layers is so far still inferior to that of the silicon dioxide and some other oxide films. There are also reproducibility problems. For this reason, a diagnostics of thin fluorides in each individual case becomes a task of primary importance.

The initial understanding of electrical behavior of any metal-insulator-semiconductor (MIS) structure can be attained using capacitance-voltage (CV) measurements. Electron transport through thin films is traditionally studied relying on the recorded current-voltage (IV) curves. Mathematical models were developed for MIS capacitors[8–10] helping by interpretation of the experimental data and enabling extraction of features attributed to particular phenomena. But the validity of electrical characterization may become doubtful in presence of thickness-fluctuation-related effects, since such effects can reduce an accuracy of comparison to the model. In such respect, a more sophisticated technique using photon emission from a MIS structure can be beneficial for supporting the standard electrical data, especially in case of not perfectly parameterized systems, like CaF_2/Si.

In this work, the CV-technique, along with the surface topography recordings by atomic-force microscope (AFM), will be used for primary control of the samples quality, and the results of electrical and luminescence measurements will be summarized. One of the main goals will be to prove the elastic tunneling injection of electrons. A loss-free, i.e., elastic, carrier transport through the CaF_2 barrier layer is evidently essential for all aforementioned potential applications.

II. SAMPLE FABRICATION; FLUORITE THICKNESS FLUCTUATION

Under investigation are the Au/CaF_2/p-Si(111) structures. The 3, 5, and 7 monolayer (1 ML = 0.315 nm) CaF_2 films were fabricated by MBE on the p-Si wafers doped to $N_A = 10^{16}\,cm^{-3}$. The lattice parameter of Calcium Fluoride (0.546 nm) is well-matched with that of Silicon (0.543 nm); the (111) orientation of Si substrate thermodynamically enables growth of a homogeneous CaF_2 layer.[2,11] Application of the standard Shiraki method[12] for chemical treatment of Si substrate and MBE growth at an optimized temperature of 250 °C allowed for obtaining pinhole-free films. Like in the most of works on CaF_2 MIS structures, gold was used for gate contacts (Au thickness 40 nm; diameter 80 μm). The schematically drawn configuration of the investigated device is given in Fig. 1(a).

So far the CaF_2 films have been grown exclusively on n-Si(111) substrates as most of the applications like RTD require n-type wafers. Nevertheless, the case of p-Si is also important, e.g., for field effect transistors. Moreover, as will be explained further, the p-samples are more convenient for optical studies.

The main parameters to characterize homogeneity of the insulating layers are the values of the topography root mean square (*rms*). They were extracted from the AFM images

[a]Author to whom correspondence should be addressed. E-mail: illarionov@iue.tuwien.ac.at. Telephone: +4315880136035

 © 2014 AIP Publishing LLC

[This article is copyrighted as indicated in the article. Reuse of AIP content is subject to the terms at: http://scitation.aip.org/termsconditions. Downloaded to] IP: 128.131.199.82 On: Thu, 10 Jul 2014 10:07:53

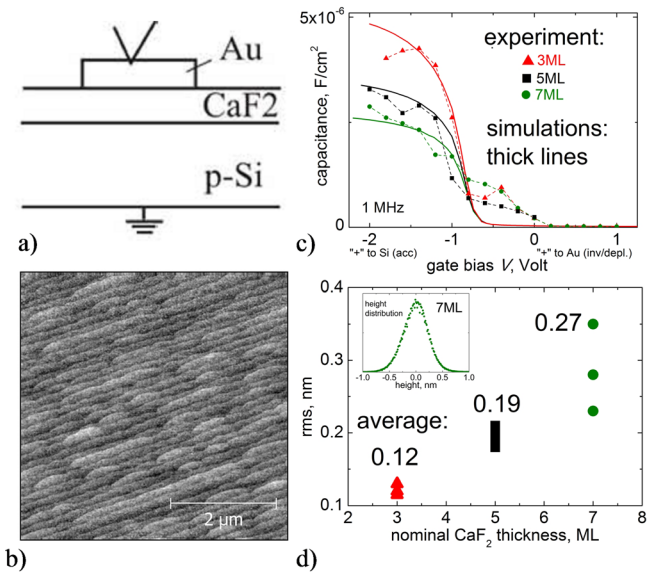

FIG. 1. (a) Device structure. (b) Example of a CaF_2 AFM topography image; total height variation ~1 nm. (c) A family of the Capacitance-Voltage curves (in simulation, the averaged *rms* value is taken for the standard deviation of CaF_2 thickness); these curves are quite usual for the tunnel-thin MIS capacitor. (d) The *rms* values as deduced from such AFM images as "b" (measured at several places) and their average for each nominal thickness. Owing to optimized fluoride growth technology, there are no pinholes and the *rms* values are rather moderate.

measured in several regions on CaF_2 surface between the gold electrodes. The *rms* is to deem equal to the standard thickness deviation σ_d. The results are represented in Fig. 1; one can see the typical surface morphology of CaF_2/Si(111) structure (1b) and the dependence between the *rms* values and nominal fluorite thickness d (1d), which demonstrates that the fluctuation is higher for thicker structures. All else equal, it is to expect that the deviation σ_d should be proportional to the square root of d (the thickness dispersion of a pile containing N "independent" monolayers must, theoretically, be proportional to N; so the standard thickness deviation will be $\sim N^{1/2}$). Since *rms* increases more rapidly than $\sim d^{1/2}$, certain deterioration for thicker fluorides may be suggested, which is not unusual. In the literature, a detailed study on the role of thickness non-uniformities has been given for oxide case in Ref. 13; although in the most researches, the problem is simply silenced.

Due to the optimized growth technology, the *rms* values are rather low. However, unlike in the work[2] on the CaF_2/n-Si system where σ_d, was under 0.1 nm and could be neglected, they have now to be taken into account in simulations. One of the reasons why the sigma values are here not as small as in Ref. 2 may be a little bit larger miscut angle of the wafer used; the nonzero angle results in the nearly parallel terraces as seen in the AFM image. Considering the potential application of CaF_2 layers in RTDs, a minimization of miscut angle must be further paid attention to, as thickness fluctuation will compromise the peak-to-valley ratio. Note that in previous studies, the question on the *rms* for fluoride layers often remained hidden under a more severe non-homogeneity problem of pinholes. In the present case, there are no pinholes; this fact is also reflected by a Gaussian form of the height distribution, inset to Fig. 1(d) (with pinholes, an additional hump left from the maximum would have appeared).

III. ELECTRICAL CHARACTERIZATION; MODELING

Fig. 1(c) shows typical high-frequency (1 MHz) CV-characteristics measured on the fabricated CaF_2 MIS samples. These measurements were performed using the standard RLC meter. (To exclude a mechanical damage of the electrodes, the voltage in all measurements was fed to the Au using an AFM tip with conductive cantilever.) The theoretical curves were simulated considering quantization effects and are presented on the same plot. All characteristics show quasi-saturation for accumulation, i.e., at negative V, and a very low capacitance for the deep-depletion polarity. An effect of CaF_2 thickness is clearly observable and reasonably agrees to the simulated value. Certain capacitance fall-out for the thinnest sample is due to large leakage and was observed also for thin samples with silicon dioxide.[14] An excess capacitance near the zero voltage is owing to the surface states whose analysis may need separate study.

The measurements of the current-voltage characteristics were carried out at the NT-MDT AFM-based probe station connected to the electrical scheme with Keithley 4200-SCS unit served as a voltage source and ammeter. Measured static IV curves for both polarities are shown in Fig. 2. Here, similar to Fig. 1(c), a negative voltage V corresponds to the accumulation mode of the examined CaF_2 MIS structures. To be more exact, accumulation spans not left from zero, but only left from the bias of about −0.7 V due to finite flat-band voltage; however, main attention will be further paid to the range of higher $|V|$ where this remark does not matter.

There is a clear asymmetry in all curves. For positive bias, the current saturates due to the lack of minority carriers. Such a feature is known from the theories of MIS systems and was many times confirmed in measurements, e.g., on the

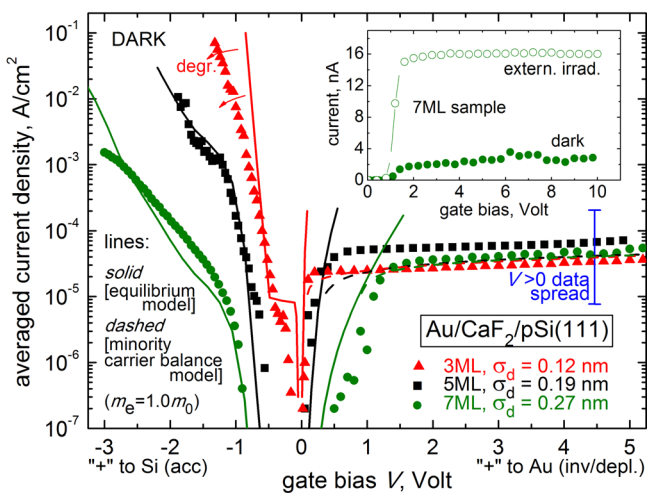

FIG. 2. Static current-voltage curves of the fabricated MIS structures with the CaF_2 insulator. The simulation is done with the physical (not fitted) barrier parameters and the thickness deviation data from Fig. 1(d). The used model suggests elastic tunneling injection. Current saturation for $V > 0$ is due to lack of minority carriers. If extra electrons are being generated due to external irradiation (*inset*), the current will be larger.

[This article is copyrighted as indicated in the article. Reuse of AIP content is subject to the terms at: http://scitation.aip.org/termsconditions. Downloaded to] IP: 128.131.199.82 On: Thu, 10 Jul 2014 10:07:53

structures with silicon dioxide (see classical papers[15,16] or later studies[9,10]). For the forward bias, i.e., accumulation, there is a quasi-exponential increase of the current with the voltage. For $V<0$, the current is very sensitive to the insulator thickness and its change even by 2 ML is unequivocally discernable. Because the main part of the applied negative bias drops across the dielectric layer, this bias regime is much more suitable for the study if aiming at deeper understanding of the transport processes within the barrier layer, rather than of a behavior of MIS structure in general. For $V<0$, otherwise than for $V>0$, the injection condition (insulator voltage) is strongly dependent on the $|V|$ value and may be widely varied, that enables a detailed study.

An overload of the sample causes degradation of the insulator layer. For the 3ML samples, it may occur even at low bias, as revealed by some current decrease in progress of measurement under accumulation polarity (Fig. 2), maybe due to a burnout of the thinnest spots leading to an increase of the effective thickness of the insulator.

In the inset to Fig. 2, the effect of photosensitivity of the CaF_2 MIS structures at $V>0$ is shown. Irradiation by an external light with a photon energy exceeding the Si bandgap (red laser was used) results in a noticeable current increase, because the absorbed light generates additional minority carriers. This property is also known for the more casual SiO_2-based MIS structures.

Fig. 2 is also completed by the simulated current-voltage characteristics obtained within an equilibrium (unique Fermi level in the substrate) approach commonly employed for MISFETs. However, at positive V, this approach does not work and the leakage-supply balance of minority carriers needs to be accounted for.[9] Then, a clear current plateau is obtained whose value may be adjusted by varying the generation rate. In fact, in this range, there may be large sample-to-sample or series-to-series spread because much depends on the purity of the silicon wafer and, in part, of an insulating/semiconductor interface. The range of a measured plateau current in the present experiment is marked with an error bar in the figure.

The simulation technique was relying on the regular models of a MIS tunnel structure. Such models allow for predicting a voltage partitioning and the currents flowing between the metal and conduction/valence band of Si (j_e, j_h). Although the barrier parameter values for calcium fluoride are not yet unequivocally established, some set can be found in literature:[2,17] the electron effective mass in CaF_2 is $m_e=1.0m_0$, the Si/CaF_2 conduction band offset is $\chi_e=2.38\,eV$, and the Au/CaF_2 barrier is $\chi_m=2.63\,eV$. A non-homogeneity of the insulating layers has been accounted for adopting Gauss distribution of the insulator thickness with dispersion $\sigma_d \approx rms$ extracted from AFM images. Note that the effect of finite σ_d on the current is much stronger than that on the capacitance. Below, without comprehensively recalling the theory of MIS tunnel structures, the key details for the $Au/CaF_2/p\text{-}Si(111)$ system will be touched. For brevity, the currents are written omitting the external Gauss-weighting integration over the local fluoride thickness.

Both components j_e, j_h contain "continuous" part involving the three-dimensional states in Au and Si, and either component also a "discrete" part from/into the quantum levels in the near-interface well. The "continuous" current reads

$$j_{e|h}^{cont}=\frac{q}{4\pi^3\hbar}\cdot\int\Delta f(E)dE\int\int T(E,k_\perp^2)d^2\vec{k}_\perp. \tag{1}$$

Here, $k_\perp$ is a transverse to the tunneling direction z wave vector of an electron, E is its energy, and Δf is the Fermi function difference in gold and silicon. The transfer probability is

$$T(E,k_\perp^2)=\exp\left[-2\hbar^{-1}\int\sqrt{2m_e\left(E_{cI}(z)-E+\hbar^2k_\perp^2/2m_e\right)}dz\right] \tag{2}$$

with $E_{cI}(z)$ labeling the CaF_2 conduction band profile. The use of Eq. (1) requires knowledge of the full Si band structure; at the same time, profit might be doubtful due to inaccuracy with the barrier parameters. For tunneling into/from a parabolic band near the minimum/maximum in a no-transverse-shift ($k_{0\perp}=0$) case, Eq. (1) is converted into the popular formula

$$j_{e|h}^{cont}=\frac{4\pi q\nu_v m_\perp}{h^3}\int\Delta f(E)dE\int T(E,E_\perp)dE_\perp, \tag{3}$$

where ν_v is valley degeneracy and $E_\perp$ is the "transverse" energy in Si ($E_\perp=(\hbar k_\perp)^2/2\,m_\perp$, $m_\perp$ is the effective mass in interface plane). Equation (3) applies to Si valence band. As for conduction bands, for Si(100), it is valid for two of the 6 valleys. For Si(111), it is relevant for one (in fact, for two but at the Brillouin-zone-border) of the L-minima.

In our earlier work,[18] the known expression (3) was used also for tunneling from/into the lowest valleys of Si(111): at the place of $T(E, E_\perp)$, the probability $T^*=\langle T(E, k_\perp{}^2(E,E_\perp,\varphi))\rangle_\varphi$ averaged over states with the given E, $E_\perp$ pair was inserted. For $E-E_{c0}<1\,V$, where E_{c0} is the Si conduction band edge at the CaF_2/Si interface, this procedure yields very close result to that of Eq. (1). The striking aspect is that for tunneling near the lowest minima, transmission probability is reduced due to conservation of a large transverse momentum (for the minima, $k_{0\perp}\neq 0$). In Ref. 18, the discrete current part, not written-out above, has also been treated. In this study, the routine of Ref. 18 is exercised, with an extension relevant for electron injection with the energies of 1–2 eV at $V<0$. Namely, electron transport into the L-minimum for $E-E_{c0}>E_L=0.9\,eV$ is now regarded

$$j_e=\frac{4\pi q}{h^3}\cdot\left[6m_\perp\int_{E_{c0}}^{+\infty}\Delta f(E)dE\int_0^{E-E_{c0}}T^*(E,E_\perp)dE_\perp+m_{\perp L}\times\int_{E_{c0}+E_L}^{+\infty}\Delta f(E)dE\int_0^{E-E_{c0}-E_L}T(E,E_\perp)dE_\perp\right]. \tag{4}$$

As the transverse wave vectors in the latter process are small, the probability T increases. So, there appears extra current rise in simulation (s. left from about $-2.5\,V$, case 7 ML).

[This article is copyrighted as indicated in the article. Reuse of AIP content is subject to the terms at: http://scitation.aip.org/termsconditions. Downloaded to] IP: 128.131.199.82 On: Thu, 10 Jul 2014 10:07:53

However, this rise does not look abrupt as it occurs on the background of a contribution of the first term in Eq. (4). The upper integral limit of E is formal as the integrands rapidly decrease above the metal Fermi energy E_{Fm}.

The results given in Fig. 2 demonstrate a satisfactory agreement between the measured IV characteristics and the simulation data. It is also clearly seen that despite non-zero *rms* of the insulating layers the thickness effect takes place in accumulation mode, as well as in inversion-depletion mode at low V, i.e., before the current plateau. In other words, the current value is higher for the structures with smaller nominal thickness of CaF_2 layer as it should be in a case of tunnel mechanism of charge transport. So far, nothing special was observed in the range of activation of tunneling in the L-minimum, may be because that bias range is already damaging. The non-trivial aspects of Si band structure might become more plausible for MIS diodes with thicker CaF_2 where the attainable energies are higher.

Although this point is often not emphasized, the tunnel models presume an elastic transport of the electrons, so that the mentioned coincidence attests the process of transport without losses. Furthermore, in an "elastic" case, the energy distribution of transported carriers peaks sharply near E_{Fm}. As already said, for many applications, it is important that the electrons be not just "injected" but entered the semiconductor with a determined energy. Beyond the RTDs, elastic injection is also essential for the impact-ionization-based devices, such as Auger transistor[19] where the injected carriers should produce new electron-hole pairs. By the way, for the $Al/SiO_2/n$-Si systems, the adequate interrelation between the ionization characteristics and the applied voltage may serve as indicator of an injection without scattering, because the quantum yield as function of energy is relatively well-known.

Characterization of a carrier injection by IV-method is easy and convenient, but it reliably works only for the widely used material combinations for which the barrier parameters are established and there is no risk to get agreement due to the occasional combination of doubtful values. That the MIS structure is not well parameterized does not speak for its bad quality; but in this case, additional methods of injection energy characterization are desirable. This concerns also CaF_2.

IV. OPTICAL CHARACTERIZATION

As a supplementary and, one can say, advanced method of injection diagnostics, detection of light emission from a MIS structure was used. Such luminescence-aided characterization of the $Au/CaF_2/p$-Si system was partially made in our earlier work.[20] For this reason, here, only an essence is presented at the amount necessary in context of general diagnostics. Nevertheless, since the phenomenon of hot-carrier luminescence from Si[21] is not widely known so far, some physical aspects of it will still be recalled. What is commonly known is that a silicon device, also a MIS system, can emit light with a near-bandgap photon energy[22] (left inset to Fig. 3).

Electrons injected into Si at $V<0$ (right inset) are hot and may be engaged in different kind optical transitions:

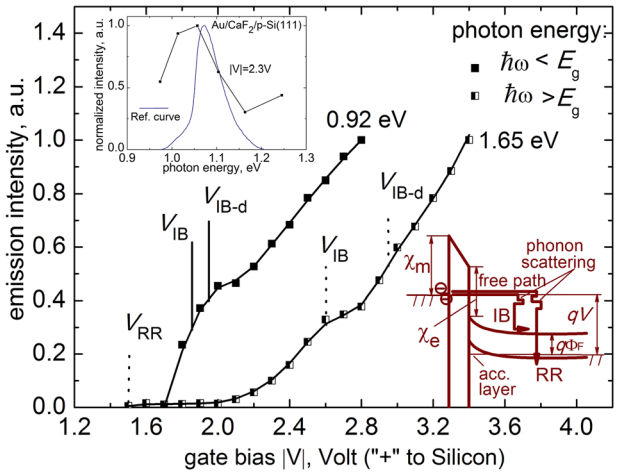

FIG. 3. Intensity of a hot-electron-injection-induced radiation from the $Au/CaF_2/p$-Si structure within the narrow spectral interval around the indicated photon energy—there are features showing onsets of different light-emission mechanisms. *Insets*: left—fragment of the radiation spectrum measured near the Si band-gap (a peak due to thermalized carriers); right—band diagram ($V<0$) with a schematic of carrier energy evolution processes.

radiative recombination (RR) and intraband (IB) photon emission. This is an additional energy-relaxation process, along with the more probable phonon scattering. The transitions take place at a mean free path distance ($L\sim 10$ nm) exceeding the band-bending accumulation region width ($\sim$2–3 nm) in p-Si. Assuming elastic transport in CaF_2, the electrons will reach the mean free path distance with an energy close to the metal Fermi level energy $E_{\mathrm{inj}}=E_{\mathrm{Fm}}$ and otherwise E_{inj} will be lower. In case of elastic injection, the activation voltages of each luminescence mechanism can be estimated as

$$qV_{RR}=\hbar\omega-q\Phi_F \tag{5}$$

and

$$qV_{\mathrm{IB}}=\hbar\omega-q\Phi_F+E_g \tag{6}$$

with $q\Phi_{\mathrm{F}}$ being the Si Fermi level, respectively, to $E_{c\infty}$. Here, $\hbar\omega$ denotes the energy of detected photons. Both RR and IB optical transitions can be classified down into the direct and indirect ones. The threshold for a direct IB luminescence,[23,24] $qV_{\mathrm{IB\text{-}d}}$, is higher than qV_{IB} and can be calculated considering the full Si band structure

$$qV_{\mathrm{IB\text{-}d}}(\hbar\omega)=E|_{\mathrm{Edir(E)}=\hbar\omega}+q\Phi_F, \tag{7}$$

where E_{dir} is the maximum direct-transition energy[23] among all states with the given energy $E=E_{\mathrm{inj}}-E_{c\infty}$ ($E_{c\infty}$ is the bulk-Si conduction band edge). Note that for MIS structures on n-Si, no any thresholds could be expected because of the smearing effect of the field in the depletion region.

The positions of thresholds for all kinds of radiative transitions are independent on the type of insulator and the barrier parameters. They can be calculated knowing only the position of Fermi level in the substrate which is defined by acceptor concentration N_{A}. The optical characterization technique relying on these concepts allows attestation of

[This article is copyrighted as indicated in the article. Reuse of AIP content is subject to the terms at: http://scitation.aip.org/termsconditions. Downloaded to] IP: 128.131.199.82 On: Thu, 10 Jul 2014 10:07:53

elastic/inelastic electron injection processes even for not perfectly parameterized systems.

The measurements of optical characteristics of the Au/CaF_2/p-Si structures were performed using a home-built Photon Emission Microscopy system.[25] The optical signal has been detected with two detectors: Pixis 1024BR_Excelon for a spectral range 500–900 nm and Xenics Xeva-1200 for 900–1500 nm. The intensity at a targeted wavelength (λ) was measured as a difference of the detector counts obtained with two long-pass filters having close edge wavelengths λ_1, λ_2 surrounding λ. The photon energy is then evaluated as $\hbar\omega = 2\pi\hbar c/\lambda$ and the presence of luminescence thresholds is analyzed.

In Fig. 3, the intensities normalized to a value of current J are plotted against the bias voltage V for $\hbar\omega < E_g$ and $\hbar\omega > E_g$. These data refer to the 5ML sample, but very similar results are obtained for any CaF_2 thickness. One can see that the thresholds positions are close to their estimated values. For example, the intensity vs. voltage curve measured with the 700 and 800 nm edged filters (on average, $\lambda = 750$ nm, i.e., $\hbar\omega = 1.65$ eV) exhibits $V_{RR} \approx 1.5$ V, $V_{IB} \approx 2.6$ V, and $V_{IB\text{-}d} \approx 2.94$ V. However, for a sub-E_g photon energy, there is no any RR contribution. So in the curve for a 1300–1400 nm wavelength range ($\hbar\omega = 0.92$ eV), only the IB thresholds $V_{IB} \approx 1.85$ V and $V_{IB\text{-}d} \approx 1.95$ V can be found. Similar values can be obtained from the mentioned above formulas with $q\Phi_F \approx 0.95$ eV and $E_g \approx 1.12$ eV. This just says that a transport of electrons, at least in its substantial part, is an elastic transport what confirms and solidifies the electrical results described above. Note that both selected values of photon energy were far enough from the bandgap of Si. In such conditions, all radiative transitions are related to the injection of hot electrons from the gold electrode into Si substrate that is especially important for optical characterization of the injection properties of insulating films.

Oppositely, the transitions with $\hbar\omega \approx E_g$ are mostly due to the RR of thermalized electrons in Si (Refs. 22 and 23) and, as already mentioned, a near-E_g recombination peak appears (Fig. 3, left inset). In our measurements, this peak is slightly distorted, as compared with its reference form–it is because we have not a RR contribution of thermalized carriers alone, but also a hot-electrons-related RR and IB in that range. Therefore, no drop of intensity down to zero outside the peak is expected. As for the shift of the maximum, it might be due to Joule heating. These details are not very important in context of optical characterization. However, one should anyway understand that if the testing measurements are performed for photon energies too close to E_g, the thresholds may be severely masked or difficult to attribute.

V. CONCLUSION

Using different methods, namely AFM topography recording, measurement of the CV-curves, analysis of the current-voltage characteristics and measurement of the light-emission spectra–the progress in understanding physical properties of thin epitaxial fluorite layers has been demonstrated. For the first time, MIS structures with CaF_2 on p-Si wafer were studied in detail. Especially, non-dissipative electron tunneling through the CaF_2 films was confirmed with both electrical and optical characterizations. The observed behavior evidences that despite some thickness fluctuations in the insulating layers, elastic tunneling remains the transport mechanism in the examined Au/CaF_2/p-Si structures. This means that crystalline quality and injection capability of the grown calcium fluoride layers are rather good. Generally, the obtained results are essential for applications of the MIS structures with CaF_2 as a hot electron injector, and especially in context of the resonant tunneling diodes. To some extent, CaF_2 may be also important in a number of other applications, e.g., it can be used as a gate insulator in FETs.

ACKNOWLEDGMENTS

The authors are grateful to D. V. Isakov, Y. Zhang, B. P. Ng, and S. W. Kok from SIMTech for their collaboration and to European Commission (Erasmus Mundus and ONDA Project FP7-PEOPLE 2009-IRSES-247518) for the financial support.

[1]C. Deiter, M. Bierkandt, A. Klust, C. Kumpf, Y. Su, O. Bunk, R. Feidenhans'l, and J. Wollschläger, Phys. Rev. B **82**, 085449 (2010).
[2]M. I. Vexler, N. S. Sokolov, S. M. Suturin, A. G. Banshchikov, S. E. Tyaginov, and T. Grasser, J. Appl. Phys. **105**, 083716 (2009).
[3]M. Watanabe, Y. Iketani, and M. Asada, Jpn. J. Appl. Phys., Part 2 **39**, L964 (2000).
[4]M. Watanabe, T. Funayama, T. Teraji, and N. Sakamaki, Jpn. J. Appl. Phys., Part 2 **39**, L716 (2000).
[5]K. Sadakuni-Makabe, M. Suzuno, K. Harada, H. Akinaga, and T. Suemasu, Jpn. J. Appl. Phys., Part 1 **49**, 060212 (2010).
[6]T. Sunohara, K. Kobayashi, M. Umada, H. Yanagihara, E. Kita, H. Akinaga, and T. Suemasu, Jpn. J. Appl. Phys., Part 2 **44**, L715 (2005).
[7]T. Waho and F. Yanagawa, IEEE Electron Devices Lett. **9**, 548 (1988).
[8]M. I. Vexler, N. Asli, A. F. Shulekin, B. Meinerzhagen, and P. Seegebrecht, Microelect. Eng. **59**, 161 (2001).
[9]M. I. Vexler, S. E. Tyaginov, Yu. Yu. Illarionov, Y. K. Sing, A. D. Shenp, V. V. Fedorov, and D. V. Isakov, Semiconductors **47**, 686 (2013).
[10]A. Schenk, *Advanced Physical Models for Silicon Device Simulations* (Springer, Wien, NY, 1998), Chap. 5.
[11]L. J. Schowalter and R. W. Fathauer, Crit. Rev. Solid State Mater. Sci. **15**, 367 (1989).
[12]A. Ishizaka and Y. Shiraki, J. Electrochem. Soc. **133**, 666 (1986).
[13]B. Majkusiak and A. Strojwas, J. Appl. Phys. **74**, 5638 (1993).
[14]W. K. Henson, K. Z. Ahmed, E. M. Vogel, J. R. Hauser, J. J. Wortman, R. D. Venables, M. Hu, and D. Venables, IEEE Electron Devices Lett. **20**, 179 (1999).
[15]M. A. Green, F. D. King, and J. Shewchun, Solid State Electron. **17**, 551 (1974).
[16]J. Shewchun, M. A. Green, and F. D. King, Solid State Electron. **17**, 563 (1974).
[17]*Crystals with the Fluorite Structure: Electronic, Vibrational, and Defect Properties*, edited by W. Hayes (Clarendon Press, Oxford, 1974).
[18]M. I. Vexler, Yu. Yu. Illarionov, S. M. Suturin, V. V. Fedorov, and N. S. Sokolov, Phys. Solid State **52**, 2357 (2010).
[19]E. V. Ostroumova and A. A. Rogachev, Semiconductors **28**, 793 (1994).
[20]Yu. Yu. Illarionov, M. I. Vexler, V. V. Fedorov, S. M. Suturin, and N. S. Sokolov, Thin Solid Films **545**, 580 (2013).
[21]J. Bude, N. Sano, and A. Yoshii, Phys. Rev. B **45**, 5848 (1992).
[22]N. A. Sobolev, in *Advances in Light Emitting Materials*, edited by B. Monemar *et al.* (Trans Tech Publications, 2008), pp. 79–100.
[23]N. Asli, M. I. Vexler, A. F. Shulekin, P. D. Yoder, I. V. Grekhov, and P. Seegebrecht, Microelectr. Reliab. **41**, 1071 (2001).
[24]E. Cartier, J. C. Tsang, M. V. Fischetti, and D. A. Buchanan, Microelectr. Eng. **36**, 103 (1997).
[25]Y. Ding, D. P. Poenar, and D. V. Isakov, in *19th IEEE International Symposium on the Physical and Failure Analysis of Integrated Circuits (IPFA)* (Singapore, 2012), pp. 1–6.

[This article is copyrighted as indicated in the article. Reuse of AIP content is subject to the terms at: http://scitation.aip.org/termsconditions. Downloaded to] IP: 128.131.199.82 On: Thu, 10 Jul 2014 10:07:53